

Competing Ordered States in Bilayer Graphene

Fan Zhang^{1,*}, Hongki Min², and A.H. MacDonald³

¹ *Department of Physics and Astronomy, University of Pennsylvania, Philadelphia, PA 19104, USA*

² *Department of Physics and Astronomy, Seoul National University, Seoul 151-747, Korea*

³ *Department of Physics, University of Texas at Austin, Austin TX 78712, USA*

(Dated: June 25, 2018)

We use a perturbative renormalization group approach with short-range continuum model interactions to analyze the competition between isotropic gapped and anisotropic gapless ordered states in bilayer graphene, commenting specifically on the role of exchange and on the importance of spin and valley flavor degeneracy. By comparing the divergences of the corresponding susceptibilities, we conclude that this approach predicts gapped states for flavor numbers $N = 1, 2, 4$. We also comment briefly on the related gapped states expected in chiral (ABC) trilayer graphene.

PACS numbers: 71.10.-w, 71.10.Hf, 71.10.Pm

I. INTRODUCTION

In chirally stacked few layer graphene systems¹⁻⁵ two sublattice sites, one in the top layer and one in the bottom layer, are disconnected from the near-neighbor interlayer hopping network and partially isolated. This geometric feature leads to a gapless semiconductor with weakly dispersive conduction and valence band edges, and therefore to an enhanced role for electron-electron interactions^{4,5}. The low-energy sublattice degree-of-freedom in chirally stacked N layer graphene can be viewed as a $S = 1/2$ pseudospin, with \uparrow -pseudospins corresponding to top layer states and \downarrow -pseudospins to bottom layer states. In this language the conduction and valence band eigenstates at wavevector $\mathbf{q} = q(\cos\phi_{\mathbf{q}}, \sin\phi_{\mathbf{q}})$ have $\hat{x}-\hat{y}$ plane pseudospin orientations, *i.e.* they have equal weight in top and bottom layers, and azimuthal angles $N\phi_{\mathbf{q}} + \pi$ and $N\phi_{\mathbf{q}}$ respectively. A number of years ago we predicted⁶ on the basis of an unrestricted Hartree-Fock mean-field-theory that these circumstances would lead to ground states with pseudospin order, and in particular to a state in which the pseudospins rotate out of the $\hat{x}-\hat{y}$ plane by a k -dependent polar angle toward either the north or the south pole, breaking layer-inversion symmetry⁷ and inducing a gap⁸ in the charged excitation spectrum. Recent bilayer experimental work⁹⁻¹⁵ has yielded clear evidence for broken symmetry states, although a consensus on the character of their order has not yet been achieved. At the same time a substantial body of theoretical work^{5,8,16-37} has used a variety of different approaches to study bilayer graphene. The general consensus of this work is that the ground state is a pseudospin ferromagnet. It has become clear however that because of quantum fluctuations that are not captured by mean-field theory, the gapped state competes closely with a gapless anisotropic state in which the net pseudospin alignment is in the $\hat{x}-\hat{y}$ plane, not the \hat{z} direction. This paper addresses that competition.

As we will explain in more detail later, some features of the bilayer graphene system present awkward obstacles to theory. First among these is the property that the conduction and valence bands are weakly dispersive only

over the small part of the Brillouin zone where inter-layer tunneling plays an essential role. Elsewhere in the Brillouin zone interaction effects are expected to be similar to those in single-layer graphene, producing strong quasi-particle velocity enhancements,³⁸⁻⁴⁰ and spectral weight rearrangements,^{41,42} but not order. The small number ($\sim 10^{-4}$) of π -electrons per carbon atom in the strongly correlated region of momentum space is an obstacle for theories of the ordered state that are based primarily on a lattice model of graphene. The narrow momentum-space distribution of the most important virtual states also creates difficulties for continuum models because it makes the physics sensitive to the long-range of the Coulomb interaction. In this paper we report on calculations in which lattice effects are completely ignored and the long-range of the Coulomb interaction is not treated explicitly. In our view the continuum approach we use is strongly motivated by the low-density of strongly correlated electrons. Our use of short-range interactions can be crudely justified by appealing to screening considerations, and arguing that the momentum-independent interaction parameters we use represent an average over the relevant portion of momentum space. Although not fully rigorous in this sense, we believe that the conclusions we reach by following this approach systematically are nevertheless valuable and consistent with recent experimental work.^{9-15,43}

This paper elaborates on ideas presented in a series of closely related earlier papers^{8,17,19,22,31} in which the ground state is estimated on the basis of perturbative renormalization group (PRG) calculations. These calculations differ among themselves most essentially in the approximate ways they account for lattice scale physics and long-range interactions. In Section II we briefly describe the model we study and restate some identities and observations that are useful in developing its perturbation theory. Section III presents new results for the PRG interaction flows of this model, emphasizing the role of exchange interactions between electrons with the same spin and valley states and commenting on the flavor number (N) dependence of the interaction parameter flows. In Section IV we explain how the PRG pseudospin sus-

ceptibilities, whose divergences suggest the character of the low-temperature order, depend on the renormalized interaction strengths. Finally in Section V we present our conclusions and discuss the relationship of our work to experiments and to other theoretical work on this system.

II. THEORETICAL PRELIMINARIES

Bilayer graphene (BLG) is described approximately at low-energies by the $J = 2$ version of the chiral band Hamiltonian:²⁻⁵

$$\mathcal{H}_J = \sum_{\mathbf{q}\alpha\beta i} \frac{(\hbar v q)^J}{(-\gamma_1)^{J-1}} c_{\mathbf{q}\alpha i}^\dagger [\cos(J\phi_{\mathbf{q}})\sigma_{\alpha\beta}^x + \sin(J\phi_{\mathbf{q}})\sigma_{\alpha\beta}^y] c_{\mathbf{q}\beta i}. \quad (1)$$

In Eq. (1) σ are Pauli matrices which act on the (Greek) layer labels and $i = 1, \dots, N$ is a spin-valley flavor label. We have used the notation $\cos\phi_{\mathbf{q}} = \tau^z q_x/q$ and $\sin\phi_{\mathbf{q}} = q_y/q$. Here $\tau^z = \pm 1$ labels K and K' valleys located at inequivalent Brillouin zone (BZ) corners and $\mathbf{q} = (q_x, q_y)$ is wavevector measured from the BZ corner. It is convenient to perform a rotation in BLG pseudospin space⁴⁴ in the K' ($\tau_z = -1$) valley to eliminate the valley dependence of the band Hamiltonian, in order to make our discussion more concise in the following sections. The BLG chiral band Hamiltonian applies^{2,3} at energies smaller than the interlayer hopping scale $\gamma_1 \sim 400$ meV and larger than the trigonal warping scale ~ 1 meV. We discuss the important role of trigonal warping in the band-structure later. The physics discussed in this paper applies to bilayers when $J = 2$ and partly generalizes to J -layer chirally (ABC) stacked graphene multilayers,^{4,43,45,46} although the chiral band Hamiltonian \mathcal{H}_J applies over narrower ranges of energy for larger J . We will focus our attention on the $J = 2$ case hereafter.

\mathcal{H}_2 can be viewed as specifying a momentum \mathbf{q} -dependent effective magnetic field that acts on the bilayer layer-pseudospin degree-of-freedom:

$$\mathcal{H}_2 = -\mathbf{B} \cdot \boldsymbol{\sigma}, \quad (2)$$

where $|\mathbf{B}| = \xi_{\mathbf{q}} = \hbar\omega_{\mathbf{q}} = \hbar^2 q^2 / 2m^*$ with $m^* = \gamma_1 / (2v^2)$, and the orientation angle of \mathbf{B} is $2\phi_{\mathbf{q}}$. The corresponding Matsubara Green's function is

$$\mathcal{G}_{\mathbf{q}}(i\omega_n) = [i\omega_n - \mathcal{H}/\hbar]^{-1} = \mathcal{G}_{\mathbf{q}s}(i\omega_n) + \mathcal{G}_{\mathbf{q}t}(i\omega_n) \mathbf{n} \cdot \boldsymbol{\sigma} \quad (3)$$

where

$$\mathcal{G}_{\mathbf{q}s,t}(i\omega_n) \equiv \frac{1}{2} \left(\frac{1}{i\omega_n - \omega_{\mathbf{q}}} \pm \frac{1}{i\omega_n + \omega_{\mathbf{q}}} \right), \quad (4)$$

and $\mathbf{n} = -(\cos 2\phi_{\mathbf{q}}, \sin 2\phi_{\mathbf{q}}, 0)$. Note that $\mathcal{G}_s(-i\omega_n) = -\mathcal{G}_s(i\omega_n)$ whereas $\mathcal{G}_t(-i\omega_n) = \mathcal{G}_t(i\omega_n)$. When expressed explicitly as a 2×2 matrix,

$$\mathcal{G}(i\omega_n) = \begin{pmatrix} \mathcal{G}_s(i\omega_n) & -\mathcal{G}_t(i\omega_n)e^{-2i\phi_{\mathbf{q}}} \\ -\mathcal{G}_t(i\omega_n)e^{2i\phi_{\mathbf{q}}} & \mathcal{G}_s(i\omega_n) \end{pmatrix}. \quad (5)$$

The off-diagonal *triplet* component captures processes in which electrons propagate between layers; its momentum-orientation dependent phase factor plays an essential role in the one-loop PRG calculations described in the next section. The frequency sums which appear in loop diagrams are readily evaluated:

$$\begin{aligned} \frac{1}{\beta\hbar^2} \sum_{\omega_n} \mathcal{G}_{\mathbf{q}s,t}^2(i\omega_n) &= \mp \frac{\tanh(\beta\xi_{\mathbf{q}}/2)}{4\xi_{\mathbf{q}}} \xrightarrow{T \rightarrow 0} \mp \frac{1}{4\xi_{\mathbf{q}}}; \\ \frac{1}{\beta\hbar^2} \sum_{\omega_n} \mathcal{G}_{\mathbf{q}s}(i\omega_n)\mathcal{G}_{\mathbf{q}t}(i\omega_n) &\xrightarrow{T \rightarrow 0} 0. \end{aligned} \quad (6)$$

These two results express the property that fluctuations involve interband transitions. In the PRG each loop diagram is multiplied by appropriate interaction constants (discussed below) and then integrated over momentum labels near the model's flowing cutoff Λ :

$$\int_{\Lambda/s < q < \Lambda} \frac{d^2\mathbf{q}}{(2\pi)^2} \frac{\tanh(\beta\xi_{\mathbf{q}}/2)}{4\xi_{\mathbf{q}}} \xrightarrow{T \rightarrow 0} \frac{1}{2} \nu_0 \ln(s). \quad (7)$$

where $\nu_0 = m^*/2\pi\hbar^2$ is the BLG density-of-states per flavor. The second frequency sum in Eq.(6) vanishes in the long-wavelength static limit because it has contributions from intra-band particle-hole excitations only. Because $\omega_{\mathbf{q}} \propto q^2$ rather than q , this integral diverges logarithmically when the high-energy cut-off is scaled down by a factor of s . The PRG calculation is therefore very similar to the corresponding calculation for a 1DES. This rather surprising property of BLG is directly related to its unusual band structure which yields Fermi points rather than Fermi lines in neutral systems, and quadratic rather than linear dispersion.⁸

III. RG FLOW EQUATIONS

A. Number of Physical Parameters

In systems with short-range interactions, finite momentum (gradient) corrections are irrelevant in the RG flows. We therefore ignore the wave-vector transfer dependence of scattering processes starting already at the $J = 2$ chiral model's ultraviolet cut-off energy $\sim \gamma_1$. In the low-energy continuum model of BLG electrons carry spin, and both layer and valley pseudospin labels. In a scattering event, both the two incoming and two outgoing particles can therefore have one of eight labels and the general scattering function therefore has 8^4 distinct values, even when gradient corrections are ignored. The number of distinct coupling constants in the RG flow equations is much smaller, however, because many values are zero and others are related to each other by symmetry. One simplification is that interactions conserve spin and, in the continuum model, both layer and valley pseudospin at each vertex. The role of spin in our model is therefore equivalent to the role of valley. We

do however choose to allow the interaction strength between electrons in different (D) layers to be weaker than that between electrons in the same (S) layer so that the interactions are layer-pseudospin dependent.

The internal loops in the PRG calculation contain two fermion propagator (Green's function) lines. Because we seek a momentum-independent effective interaction we simplify the calculation by evaluating the coarse-graining correction to the effective interaction for the case where all incoming and outgoing electrons are at the Dirac point. (As we comment in the discussion section, this approximation is made less innocent by the layer pseudospin structure of the band eigenstates.) These propagators conserve both spin and valley pseudospin, but as we have seen above, not the layer pseudospin. From Eq.(5) we see that a phase factor⁴⁴ $e^{\pm 2i\phi_a}$ appears when a propagator transfers electrons between layers. Unless these layer transfers enter an equal number of times in each direction, the integrand in a Feynman diagram will contain a net phase factor related to chirality and vanish upon angular integration of the virtual momentum. The total layer number (the \hat{z} component of layer pseudospin) is therefore also conserved.⁴⁴ This property combined with flavor invariance limits the number of independent interaction parameters to three, two for interaction processes involving electrons in the same layer or different layers that conserve layer index, and one for interaction processes between electrons in different layers accompanied which interchange layer indices. We refer to the three distinct processes, illustrated in Fig. 1, as Γ_S , Γ_D and Γ_X respectively.

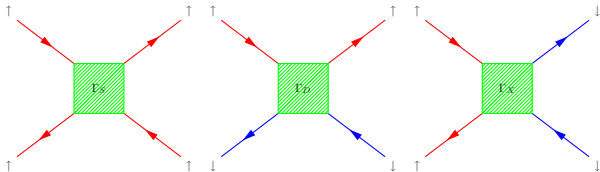


FIG. 1. (Color online) Electron-electron scattering processes for a system with a single pseudospin-1/2 degree of freedom.

If flavor invariance is broken, either due to microscopic lattice effects that violate $SU(4)$ invariance or due to broken symmetries, the number of interaction parameters increases. For example, if the bare interactions are spin and valley dependent in an arbitrary way, the number of independent *antisymmetrized* interaction parameters increases from three to ten:⁸ $\Gamma_{SSD}, \Gamma_{SDS}, \Gamma_{SDD}, \Gamma_{DSS}, \Gamma_{DSD}, \Gamma_{DDS}, \Gamma_{DDD}, \Gamma_{XSD}, \Gamma_{XDS}$ and Γ_{XDD} . In this notation the first label follows the convention explained above for the layer pseudospin dependence of the interaction, whereas the second and third labels refer to valley and spin respectively, and distinguish the interaction between particles with the same (S) or different (D) spin or valley. The number of entries in this list of interactions has been reduced by two by appealing to Fermi statistics for the case

of SS interactions, those between particles with the same spin and valley labels. In that case interchanging the labels of outgoing electrons yields an indistinguishable and canceling amplitude for particles in the same layer. Although we can choose to retain Γ_{SSS} in the RG flows, it cannot contribute to any physical observable. Similarly, since Γ_{DSS} and Γ_{XSS} are interchanged by reversing outgoing labels they differ only by a sign and it is sufficient to retain one parameter. The number of independent interacting parameters in the analysis by Vafeek²⁰ and by Lemonik *et al.*,³⁴ who impose the symmetry of the underlying BLG crystal but do not explicitly account for antisymmetrization is nine. For $SU(4)$ invariant models the number of parameters is three, but antisymmetrization allows us to retain only one coupling constant in the single flavor ($N = 1$) case, and the physical implications of the flowing interactions are more apparent if we do so.⁸ A convenient choice⁸ is to retain Γ_{DSS} . We take the view that the underlying lattice²³ is unlikely to play an important role in determining whether the broken symmetry state is gapped⁸ or gapless,^{17,22} though it is key to selecting²³ between distinct gapped states⁵ that are equivalent in an $SU(4)$ invariant model. Therefore, the number of interactions parameters that appear in the calculation described below is three in the general case with unbroken flavor invariance and one for the special case of $N = 1$.

B. RG Flow for $N = 1$

In this subsection we explore the similarities and differences between BLG and 1DES's by temporarily neglecting the spin and valley degrees-of-freedom. We choose the single effective interaction parameter to be Γ_D . A PRG analysis determines how the bare interaction at the γ_1 scale, V_D , is renormalized by integrating out the high energy fermion degrees of freedom. At one loop level the coarse-graining contributions to the effective interaction are described⁴⁷ by the three higher order diagrams labeled ZS, ZS', and BCS. The internal loops in these diagrams are summed over the high-energy labels. The main merit of the PRG is that it treats all virtual processes on an equal footing,

It is well known that in a 1DES the ZS loop vanishes while the ZS' and BCS diagrams cancel, implying that the interaction strength does not flow to large values and hence that neither the CDW repulsive interaction nor the BCS attractive interaction instabilities predicted by mean-field theories survive the quantum fluctuations they neglect. The key features of BLG order physics can be understood in terms of two properties of these one-loop diagrams; (i) the particle-particle (BCS) and particle-hole (ZS, ZS') loops have the same logarithmic divergences as in the 1DES case in spite of the larger space dimension and (ii) the ZS loop, which vanishes in the 1DES case, is finite in the BLG case and the BCS loop vanishes instead. Both of these changes are due to

the layer pseudospin triplet contribution to the single-particle Green's function as we explain below. The net result is that interactions flow to strong coupling even more strongly than in the mean-field approximation.

The key step in one-loop PRG calculations is identifying the coupling factors attached to the loop in each diagram. Since only opposite layer interactions need to be retained for $N = 1$ models, all scattering functions have two incoming particles with opposite layer labels and two outgoing particles with opposite layer labels, much like the 1DES case.⁴⁸ The external legs in the scattering function Feynman diagrams are labeled by the layer index ($T = \text{top layer}$ and $B = \text{bottom layer}$). The corresponding labels for the 1DES case^{47,48} are the chirality, R for right-going and L for left-going. We refer to these as the single-particle labels below when a comment refers to both 1DES and BLG cases.

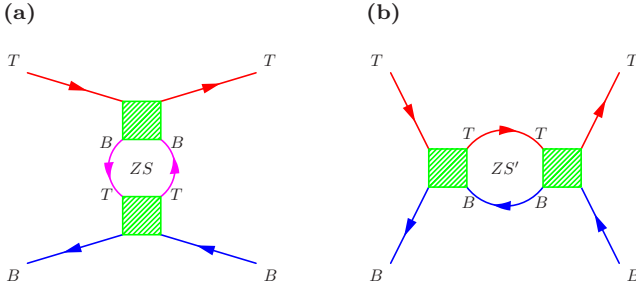


FIG. 2. (Color online) (a) ZS, (b) ZS' loop corrections in the one-loop PRG calculation.

As shown in Fig. 2(a), at the upper vertex of the ZS diagram the incoming and the outgoing T particles induce a B particle-hole pair in the loop, while the incoming and outgoing B particles at the lower vertex induce a T particle-hole pair. The ZS contribution is absent in the 1DES case^{47,48} because propagation is always diagonal in interaction labels. However, this correction survives for BLG because the single-particle Green's function has a triplet contribution (see Eq. (6)) which is off-diagonal in layer index. Here we find

$$\Gamma_D^{ZS} = \frac{\Gamma_D^2}{\beta\hbar^2} \int \frac{d^2\mathbf{q}}{(2\pi)^2} \sum_{\omega_n} \mathcal{G}_t^2(\mathbf{q}, i\omega_n) = \frac{1}{2} \Gamma_D^2 \nu_0 \ln(s). \quad (8)$$

The ZS' loop shown in Fig. 2(b) corresponds to repeated interaction between a T particle and a B hole. This is the channel responsible for the 1DES mean-field CDW instability⁴⁷ in which coherence is established between R and L particles.⁴⁸ In both 1DES and BLG cases it has the effect of enhancing repulsive interactions. Its evaluations for the two cases correspond quite closely, because this loop diagram involves only particle-propagation that is diagonal in interaction label. We find that

$$\Gamma_D^{ZS'} = -\frac{\Gamma_D^2}{\beta\hbar^2} \int \frac{d^2\mathbf{q}}{(2\pi)^2} \sum_{\omega_n} \mathcal{G}_s^2(\mathbf{q}, i\omega_n) = \frac{1}{2} \Gamma_D^2 \nu_0 \ln(s) \quad (9)$$

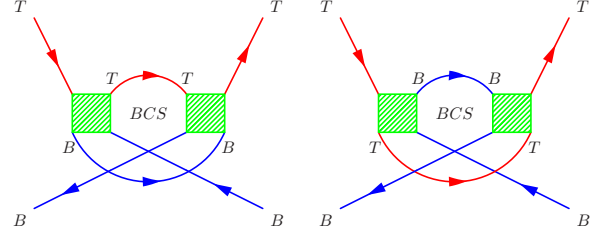


FIG. 3. (Color online) BCS (particle-particle) loop correction for singlet propagation in the one-loop PRG calculation.

The BCS channel corresponds to repeated interaction between the two incoming particles. In the 1DES case the contribution from this loop (see Fig. 3) cancels the ZS' contribution⁴⁷, leading to marginal interactions and Luttinger liquid behavior. This same kind of BCS correction for BLG reads

$$\begin{aligned} \Gamma_D^{\text{BCS}_1} &= -\frac{1}{2} \frac{\Gamma_D^2}{\beta\hbar^2} \int \frac{d^2\mathbf{q}}{(2\pi)^2} \sum_{\omega_n} \mathcal{G}_s(\mathbf{q}, i\omega_n) \mathcal{G}_s(-\mathbf{q}, -i\omega_n) \\ &\quad - \frac{1}{2} \frac{(-\Gamma_D)^2}{\beta\hbar^2} \int \frac{d^2\mathbf{q}}{(2\pi)^2} \sum_{\omega_n} \mathcal{G}_s(\mathbf{q}, i\omega_n) \mathcal{G}_s(-\mathbf{q}, -i\omega_n) \\ &= -\frac{1}{2} \Gamma_D^2 \nu_0 \ln(s). \end{aligned} \quad (10)$$

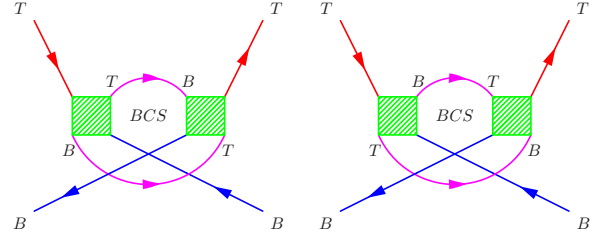


FIG. 4. (Color online) BCS (particle-particle) loop correction for triplet propagation in the one-loop PRG calculation.

In the BLG case there is an additional BCS loop contribution (see Fig. 4) in which the incoming T and B particles both change layer labels before the second interaction. This contribution is possible because of the triplet pseudospin propagation and, in light of Eq. (6), gives a BCS contribution that has the opposite sign compared to the normal contribution:

$$\begin{aligned} \Gamma_D^{\text{BCS}_2} &= -\frac{1}{2} \frac{\Gamma_D(-\Gamma_D)}{\beta\hbar^2} \int \frac{d^2\mathbf{q}}{(2\pi)^2} \sum_{\omega_n} \mathcal{G}_t(\mathbf{q}, i\omega_n) \mathcal{G}_t(-\mathbf{q}, -i\omega_n) \\ &\quad - \frac{1}{2} \frac{(-\Gamma_D)\Gamma_D}{\beta\hbar^2} \int \frac{d^2\mathbf{q}}{(2\pi)^2} \sum_{\omega_n} \mathcal{G}_t(\mathbf{q}, i\omega_n) \mathcal{G}_t(-\mathbf{q}, -i\omega_n) \\ &= \frac{1}{2} \Gamma_D^2 \nu_0 \ln(s). \end{aligned} \quad (11)$$

TABLE I. Summary of contributions from the three one-loop diagrams to Γ_D in units of ν_0 in 1DES and BLG cases.

diagrams	1DEG	BLG
<i>ZS</i>	0	$\frac{1}{2} \Gamma_D^2 \ln(s)$
<i>ZS'</i>	$u^2 \ln(s)$	$\frac{1}{2} \Gamma_D^2 \ln(s)$
<i>BCS</i>	$-u^2 \ln(s)$	0
Mean Field	$u^2 \ln(s)$	$\frac{1}{2} \Gamma_D^2 \ln(s)$
Quantum Fluctuations	$-u^2 \ln(s)$	$\frac{1}{2} \Gamma_D^2 \ln(s)$
Full One-Loop	0	$\Gamma_D^2 \ln(s)$

It follows that the BCS loop contribution is absent in the BLG case because

$$\Gamma_D^{\text{BCS}} = \Gamma_D^{\text{BCS}_1} + \Gamma_D^{\text{BCS}_2} = 0. \quad (12)$$

Therefore, at one-loop level, the renormalization of inter-layer interaction is

$$\Gamma_D^{\text{one-loop}} = \Gamma_D^{\text{ZS}} + \Gamma_D^{\text{ZS}'} + \Gamma_D^{\text{BCS}} = \Gamma_D^2 \nu_0 \ln(s). \quad (13)$$

These results and the comparison with 1DES's are summarized in Table I and imply the following RG flow equa-

tion for BLG:

$$\frac{d\Gamma_D}{\nu_0 d\ln(s)} = \Gamma_D^2. \quad (14)$$

If we follow the flows from the model's microscopic cutoff we obtain

$$\Gamma_D = \frac{V_D}{1 - V_D \nu_0 \ln(s)} \quad (15)$$

where V_D is the bare interaction. Γ_D diverges when $V_D \nu_0 \geq 1/\ln(s)$. This instability criterion is similar to the Stoner criterion for ferromagnetism.

The interaction correction to the layer pseudospin response function χ_{zz} is obtained by closing the scattering function with a σ^z vertex at top and bottom. The σ^z operator measures the charge difference between T and B layers. Because it is an effective single-particle theory, fermion mean-field theory corresponds to response function diagrams with at most a single particle-hole pair. It follows that mean-field theory in BLG is equivalent to a single-loop PRG calculation in which the BCS and ZS' channels are neglected and only the ZS channel is retained. In mean-field theory, ideal BLG has an instability to a state in which charge is spontaneously transferred between the layers which is signaled by the divergence of χ_{zz} . (χ_{xx} also diverges in mean-field theory but less strongly.) The PRG analysis demonstrates that the mean-field theory instability is enhanced by the reinforcing influence of the ZS' channel contribution. We discuss pseudospin response functions which indicate the character of the broken symmetry state further for the physically relevant $N > 1$ case in Section IV.

C. RG Flows for $N = 1, 2, 4$

Assuming $SU(4)$ invariance, the one-loop flow equations for $N > 1$ are derived in the same way as for the $N = 1$ case, except that we need to keep track of three interaction parameters, Γ_S ($\Gamma_S = \Gamma_{SDS} = \Gamma_{SSD} = \Gamma_{SDD}$), Γ_D ($\Gamma_D = \Gamma_{DDS} = \Gamma_{DSD} = \Gamma_{DDD}$) and Γ_X ($\Gamma_X = \Gamma_{XDS} = \Gamma_{XSD} = \Gamma_{XDD}$). A tedious but elementary book-keeping exercise yields the following results:

$$\begin{aligned} \frac{d\Gamma_S}{\nu_0 d\ln(s)} &= -\frac{1}{2}\Gamma_S^2 - (\Gamma_D - \Gamma_X)(\Gamma_D - \Gamma_S) - \frac{N-2}{2}(\Gamma_D - \Gamma_S)^2 + \frac{1}{2}(\Gamma_X - \Gamma_S)^2, \\ \frac{d\Gamma_D}{\nu_0 d\ln(s)} &= \frac{1}{2}\Gamma_D^2 + (\Gamma_D - \Gamma_X)(\Gamma_D - \Gamma_S) + \frac{N-2}{2}(\Gamma_D - \Gamma_S)^2 - \frac{1}{2}(\Gamma_D + \Gamma_X)^2, \\ \frac{d\Gamma_X}{\nu_0 d\ln(s)} &= (\Gamma_D - \Gamma_X)\Gamma_X - \frac{N-2}{2}\Gamma_X^2 - \frac{1}{2}(\Gamma_X - \Gamma_S)^2 - \frac{1}{2}(\Gamma_X + \Gamma_D)^2. \end{aligned} \quad (16)$$

This equation is the $SU(4)$ invariant version of the more general ten parameter flow equations derived in Ref. 8. The RG flow equations derived previously in Ref. 17 differ only in notation. The $N = 1$ case is recovered by noting that Γ_S has no physical effect for interactions among particles of the same flavor and Γ_D and Γ_X always enter

in the combination $\Gamma_D - \Gamma_X$. Defining $\Gamma_{DS} \equiv \Gamma_D - \Gamma_X$, it follows from Eqs.(16) that

$$\frac{d\Gamma_{DS}}{\nu_0 d\ln(s)} = \Gamma_{DS}^2 + \frac{N-1}{2}(\Gamma_D - \Gamma_S)^2 + \frac{N-1}{2}\Gamma_X^2, \quad (17)$$

yielding a one-parameter flow equation for the $N = 1$ case. Note that this Γ_{DS} also represents Γ_{DSS} in the $N = 4$ case.⁸

The only fixed point of these RG flow equations is the non-interacting one. The character of the broken symmetry state can be estimated by following the RG flows to strong interactions, or more reliably by following the flow equations for appropriate susceptibilities as discussed in the next section. In order to represent the property that bare same layer interactions should be slightly stronger than the bare different layer interactions and that the bare layer interchange interaction vanishes, we start the RG flow integrations from

$$V_{\text{S}} > V_{\text{D}}, \quad V_{\text{X}} = 0. \quad (18)$$

When the flows start from an interaction with these properties, the coupling constants diverge simultaneously at a finite value of $\ln(s)$, and for $N = 2, 4$ satisfy the following properties at the divergence point:

$$\begin{aligned} \frac{\Gamma_{\text{S}}}{\Gamma_{\text{D}}} &= -1, \\ \frac{\Gamma_{\text{S}}}{\Gamma_{\text{X}}} &\simeq -0.5425 \text{ (for } N = 2), \\ \frac{\Gamma_{\text{S}}}{\Gamma_{\text{X}}} &\simeq -0.2624 \text{ (for } N = 4). \end{aligned} \quad (19)$$

The value of the first ratio in Eq.(19) follows from the RG flow equation for $\Gamma_{\text{S}} + \Gamma_{\text{D}}$ which satisfies

$$\frac{d(\Gamma_{\text{S}} + \Gamma_{\text{D}})}{\nu_0 d\ln(s)} = -\Gamma_{\text{X}}(\Gamma_{\text{S}} + \Gamma_{\text{D}}). \quad (20)$$

The rate of growth of $\Gamma_{\text{S}} + \Gamma_{\text{D}}$ is proportional to $|\Gamma_{\text{X}}|$, whereas Γ_{S} and $|\Gamma_{\text{X}}|$ grow like $|\Gamma_{\text{X}}|^2$. Equivalent results in a different notation, using $2g_{0,z} = \Gamma_{\text{S}} \pm \Gamma_{\text{D}}$ and $2g_{\perp} = \Gamma_{\text{X}}$, have been derived previously by Vafeek and Yang.¹⁷ These results do not depend on the bare coupling constants as long as the physical conditions specified by Eq.(18) are satisfied. Note that the RG flows for $N = 4$ are still qualitatively different from those of the $N \rightarrow \infty$ limit.

Typical RG flows, obtained by integrating Eq.(16) numerically, are plotted in Fig. 5. We note that, when combined with the mean-field-theory of the gapped state,^{5,36} the value $\nu_0 V_{\text{S}} = 0.25$ yields values of the spontaneous gap, the critical temperature, and the carrier density at which order is absent that are consistent with some recent experimental observations^{13,14}. We therefore choose to use the bare interaction parameters $\nu_0 V_{\text{S}} = 0.25$ and $\nu_0 V_{\text{D}} = 0.22$ to illustrate typical RG flows. We find that the interaction parameters flow away from the non-interacting fixed point and diverge at a finite value of s . The instability criterion implied by the one-loop RG calculation is $\nu_0 V_{\text{S}} \simeq 0.7/\ln(s)$ for $N = 4$, i.e the instability tendency is enhanced compared to the $N = 1$ case. (Although the Γ_{S} , Γ_{D} and Γ_{X} interaction parameters do diverge at a similar value of $\ln(s)$ in the $N = 1$

case, they have no physical effect because they enter observables in the combination $\Gamma_{\text{DS}} = \Gamma_{\text{D}} - \Gamma_{\text{X}}$.) Because of the quadratic band dispersion, the ratio of the inter-layer coupling scale to the gap (γ_{\perp}/Δ) can be associated²⁶ with the square of the momentum scaling factor s at the phase transition. This yields a value of Δ on the order of 1 meV, close to the scale of the gap values seen in some experiments.^{9,10,12-14}

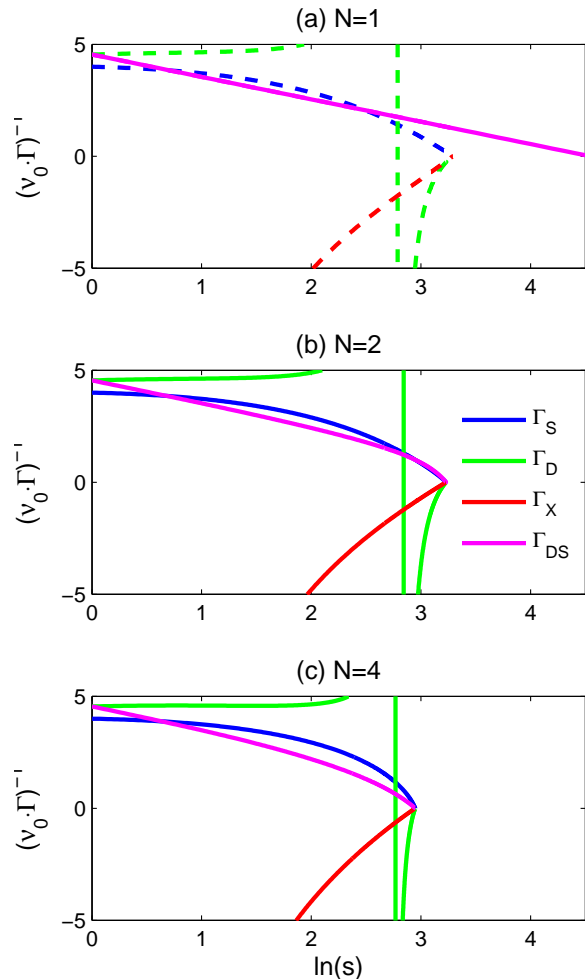


FIG. 5. (Color online) RG flows of the interaction couplings for (a) $N = 1$, (b) $N = 2$ and (c) $N = 4$. In the $N = 1$ case the dashed lines are unphysical since interactions always enter observables in the combination $\Gamma_{\text{DS}} = \Gamma_{\text{D}} - \Gamma_{\text{X}}$.

IV. SUSCEPTIBILITIES

More insight into the likely nature of the broken symmetry state which occurs in BLG can be obtained by using the PRG calculations to estimate the long wave-

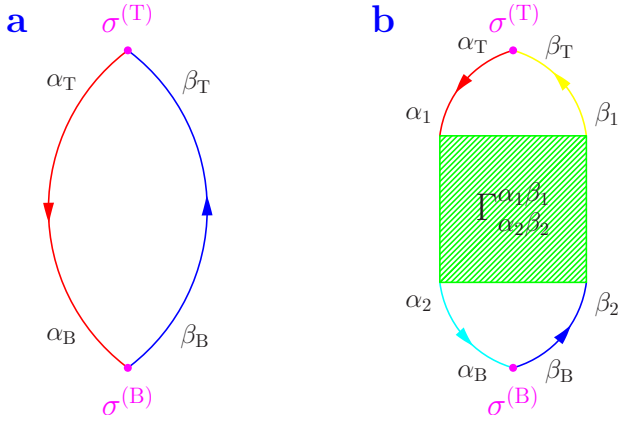


FIG. 6. (Color online) Feynman diagrams for the pseudospin susceptibilities. **(a)** The non-interacting susceptibility and **(b)** the interaction correction to the susceptibility. $T, B = x, y, z$ label layer-pseudospin components. The spin-valley flavor labels are not explicitly indicated.

length static limit of the pseudospin susceptibilities:

$$\chi_{T\gamma',B\gamma}(\mathbf{q}, i\omega) = \int_0^\beta d\tau e^{i\omega\tau} \langle T_\tau S_{T\gamma'}(\mathbf{q}, \tau) S_{B\gamma}(-\mathbf{q}, 0) \rangle, \quad (21)$$

where $T, B = x, y, z$ label layer-pseudospin components (instead of top and bottom layers) and γ', γ label either a unit matrix ($\gamma = 0$) or a generator of rotations ($\gamma = 1, \dots, 15$) in the 4-component valley-spin flavor space:

$$S_{T\gamma}(\mathbf{q}, \tau) = \sum_{\mathbf{k}} c_{\mathbf{k}+\mathbf{q}, \alpha i}^\dagger \sigma_{\alpha\beta}^{(T)} A_{i'i}^\gamma c_{\mathbf{k}, \beta i}. \quad (22)$$

A physically transparent choice⁴⁹ for the $SU(4)$ generators is to set $A_{i'i}^\gamma$ to a Pauli matrix which acts on the spin degree-of-freedom for $\gamma = 1, 2, 3$, to a Pauli matrix which acts on the valley degree-of-freedom for $\gamma = 4, 5, 6$,

$$\chi_{TB}^0 = -\int \frac{d^2\mathbf{q}}{(2\pi)^2(\beta\hbar^2)} \sum_{\omega} \sum_{\alpha_T\beta_T} \sum_{\alpha_B\beta_B} \mathcal{G}_{\alpha_B\alpha_T}(\mathbf{q}, i\omega) \sigma_{\alpha_T\beta_T}^{(T)} \mathcal{G}_{\beta_T\beta_B}(\mathbf{q}, i\omega) \sigma_{\beta_B\alpha_B}^{(B)}, \quad (23)$$

$$\chi_{TB}^{\text{int}} = -\int \frac{d^2\mathbf{q}_1 d^2\mathbf{q}_2}{(2\pi)^4(\beta\hbar^2)^2} \sum_{\omega_1\omega_2} \sum_{\text{all } \alpha\beta} \mathcal{G}_{\alpha_1\alpha_T}(\mathbf{q}_1, i\omega_1) \sigma_{\alpha_T\beta_T}^{(T)} \mathcal{G}_{\beta_T\beta_1}(\mathbf{q}_1, i\omega_1) \Gamma_{\alpha_2\beta_2}^{\beta_1\alpha_1} \mathcal{G}_{\beta_2\beta_B}(\mathbf{q}_2, i\omega_2) \sigma_{\beta_B\alpha_B}^{(B)} \mathcal{G}_{\alpha_B\alpha_2}(\mathbf{q}_2, i\omega_2). \quad (24)$$

Note that in these equations all propagators are diagonal in the implicit spin-valley flavor labels.

In the noninteracting case, the inter-flavor (D) susceptibilities vanish because the single-particle Hamiltonian is diagonal in flavor and the intra-flavor (S) susceptibilities are positive because of the band state pseudospin

and to a product of spin and valley Pauli matrices for $\gamma = 7, \dots, 15$. It follows from $SU(4)$ invariance⁴⁹ that the normal state susceptibilities in this case are $\propto \delta_{\gamma', \gamma}$ and equal for all values of $\gamma \geq 1$. Below we refer to the $\gamma = 0$ susceptibility (χ^c) as the flavor charge susceptibility and to the $\gamma \neq 0$ susceptibility (χ^s) as the flavor spin susceptibility. The conservation of particle-number in each layer at long wavelengths, explained previously, implies that $\chi_{T\gamma, B\gamma} \propto \delta_{T, B}$ and that $\chi_{x\gamma, x\gamma} = \chi_{y\gamma, y\gamma}$. Divergences in $\chi_{z,z}^c$ signal ordered states in which the charge density is transferred between layers in the same sense for all flavors, while divergences in $\chi_{z,z}^s$ signal flavor dependent layer-inversion symmetry breaking with no overall charge transfer. Divergences in $\chi_{x,x}^{c,s}$ for $T = x, y$, on the other hand imply broken symmetry states in which the phase relationship between layers is altered and rotational symmetry within the layers is broken. Broken layer-inversion symmetry states have an energy gap for charged excitations and large momentum space Berry curvatures that lead to large anomalous Hall effect contributions from individual flavors.⁵ These states will be referred to below as spontaneous quantum Hall states.⁵ The broken rotational symmetry state will be referred to below as the nematic state.

Provided that the system has a single continuous phase transition, the ordered state character can in principle be determined by identifying the pseudospin susceptibility which diverges first as temperature is lowered. Although we cannot make that determination definitively from the RG interaction strength flows, we can obtain some guidance by examining how the interaction contributions to the susceptibilities grow under the RG flows. The pseudospin response functions of interest can be related to the renormalized interactions as summarized in the Feynman diagrams of Fig. 6. Fig. 6(a) represents the non-interacting pseudospin susceptibility χ^0 and Fig. 6(b) represents the interaction correction χ^{int} . In the long wavelength static limit the explicit expressions for these susceptibilities are:

structure:

$$\begin{aligned} \chi_{zz}^{0D} &= \chi_{xx}^{0D} = \chi_{yy}^{0D} = 0, \\ \chi_{zz}^{0S} &= 2\chi_{xx}^{0S} = 2\chi_{yy}^{0S} = 2\nu_0 \ln(s). \end{aligned} \quad (25)$$

These pseudospin susceptibilities capture the contribution of momentum $\mathbf{q} = 0$ vertical interband quantum fluctuations involving states with energies measured from the Dirac point between γ_1 and γ_1/s^2 . The factor of two

difference between χ_{zz}^{OS} and χ_{xx}^{OS} demonstrates that the band state is more susceptible to a gap opening perturbation than to a nematic perturbation. This property can be understood²⁹ in terms of the pseudospin orientations of the band states; in particular a \hat{z} pseudospin effective field is perpendicular to the valence band pseudospin for all momentum orientations, so that \hat{z} direction fields always yield a strong response. On the other hand $\hat{x} - \hat{y}$ -plane pseudospin fields are not in general perpendicular to the valence band pseudospin and consequently produce a weaker response averaged over momentum orientations. The larger response to a \hat{z} pseudospin effective field is related to the well-known property of BLG that a potential difference between the top and bottom layers lead to an energy gap at the Dirac point. The corresponding charge susceptibility (density-density channel), obtained by replacing the pseudospin-field Pauli matrix by an identity matrix, vanishes because conduction and valence band states are orthogonal.

When the interactions flow to strong values, the susceptibilities are dominated by their interaction contributions. When these are included we find that

$$\begin{aligned}\chi_{zz}^{\text{D}} &= 2(\nu_0 \ln(s))^2 (\Gamma_{\text{D}} - \Gamma_{\text{S}}), \\ \chi_{xx}^{\text{D}} &= -\frac{1}{2}(\nu_0 \ln(s))^2 \Gamma_{\text{X}},\end{aligned}\quad (26)$$

$$\begin{aligned}\chi_{zz}^{\text{S}} &= 2\nu_0 \ln(s) + 2(\nu_0 \ln(s))^2 (\Gamma_{\text{D}} - \Gamma_{\text{X}}), \\ \chi_{xx}^{\text{S}} &= \nu_0 \ln(s) + \frac{1}{2}(\nu_0 \ln(s))^2 (\Gamma_{\text{D}} - \Gamma_{\text{X}}).\end{aligned}\quad (27)$$

Note that the large susceptibility in χ_{xx}^{D} is attribute to the layer interchange processes Γ_{X} while the strong divergences in $\chi_{zz,xx}^{\text{S}}$ are due to intra-flavor exchange interactions, recalling $\Gamma_{\text{D}} - \Gamma_{\text{X}} \equiv \Gamma_{\text{DS}}$ in Eq.(27).

For the $N = 1$ case there is no different-flavor response and we therefore find that near the instability

$$\chi_{zz} = 4\chi_{xx} = 4\chi_{yy}, \quad (28)$$

suggesting that a gapped spontaneous quantum Hall state is most likely.

For the physical $N = 4$ case we can relate the flavor charge and flavor spin response functions to χ^{S} and χ^{D} by examining the particular case of responses to perturbations that are diagonal in flavor index, *i.e.* perturbations proportional to s^z , τ^z or $s^z\tau^z$. We find that near the divergence point

$$\chi_{zz}^{\text{c}} = \frac{1}{4}\chi_{zz}^{\text{S}} + \frac{3}{4}\chi_{zz}^{\text{D}}, \quad (29)$$

$$\chi_{zz}^{\text{s}} = \frac{1}{4}\chi_{zz}^{\text{S}} - \frac{1}{4}\chi_{zz}^{\text{D}}. \quad (30)$$

$\chi_{xx}^{\text{c,s}}$ have the same relations to χ_{xx}^{S} and χ_{xx}^{D} . Combining Eq.(26) and Eq.(27) with the results from Eq.(19) for

$N = 4$ we find that

$$\begin{aligned}\chi_{xx}^{\text{c}} &\rightarrow +1.7805 \Gamma_{\text{S}}(\nu_0 \ln(s))^2, \\ \chi_{zz}^{\text{s}} &\rightarrow +2.4055 \Gamma_{\text{S}}(\nu_0 \ln(s))^2,\end{aligned}\quad (31)$$

$$\begin{aligned}\chi_{zz}^{\text{c}} &\rightarrow -1.5945 \Gamma_{\text{S}}(\nu_0 \ln(s))^2, \\ \chi_{xx}^{\text{s}} &\rightarrow -0.1250 \Gamma_{\text{S}}(\nu_0 \ln(s))^2.\end{aligned}\quad (32)$$

The property that all susceptibilities diverge together is an artifact of the single-loop RG calculation which becomes questionable when the scaled interactions are strong. Still, the fact that the χ_{zz}^{s} diverges most strongly suggests that the spin-channel gapped state is more likely than the charge channel nematic state. (Negative coefficients in Eq.(32) imply that one-loop interaction corrections tend to reduce the susceptibilities χ_{zz}^{c} and χ_{xx}^{s} rather than to increase them and therefore do not suggest instabilities.)

In the $N = 2$ case, which accounts for only spin or valley but not both, $\chi_{\text{T}\gamma, \text{B}\gamma'}$ the 4 dimensional γ -matrices are replaced by 2-dimensional Pauli matrices. We find that

$$\chi_{zz}^{\text{c}} = \frac{1}{2}\chi_{zz}^{\text{S}} + \frac{1}{2}\chi_{zz}^{\text{D}}, \quad (33)$$

$$\chi_{zz}^{\text{s}} = \frac{1}{2}\chi_{zz}^{\text{S}} - \frac{1}{2}\chi_{zz}^{\text{D}}, \quad (34)$$

which equally applies to the χ_{xx} channel. Combining the $N = 2$ results in Eq.(19) with Eq.(26) and Eq.(27) we obtain

$$\begin{aligned}\chi_{zz}^{\text{c}} &\rightarrow -1.1567 \Gamma_{\text{S}}(\nu_0 \ln(s))^2, \\ \chi_{zz}^{\text{s}} &\rightarrow +2.8433 \Gamma_{\text{S}}(\nu_0 \ln(s))^2, \\ \chi_{xx}^{\text{c}} &\rightarrow +0.6717 \Gamma_{\text{S}}(\nu_0 \ln(s))^2, \\ \chi_{xx}^{\text{s}} &\rightarrow -0.2500 \Gamma_{\text{S}}(\nu_0 \ln(s))^2.\end{aligned}\quad (35)$$

In both $N = 2, 4$ cases interactions favor breaking layer-inversion symmetry in the flavor spin channel and orientational symmetry in the flavor charge channel. The strongest divergence occurs for the flavor spin channel broken layer-inversion symmetry state.⁸ The $N = 1$ susceptibility and the flavor charge and spin channel susceptibilities for $N = 2, 4$ are illustrated in Fig.7 and agree with the above analytic analysis. Because χ_{zz}^{s} is always the most *positively* divergent channel we conclude that the dominant many-body effect in BLG is spin-channel spontaneous layer-inversion symmetry breaking yielding BLG states with spontaneous charge gaps. These results verify our original theoretical predictions^{6,8} and are consistent with recent experimental observations in dual-gated ultra-clean suspended BLG devices.^{9,10,13,14}

Finally, we point out that an interlayer potential breaks $SU(4)$ invariance in the $N = 4$ case, leading to a range of stability for a state in which three flavors are polarized toward one layer and one flavor toward the other layer when an ordered state appears. For instance, a possible mass term in a mean-field theory with broken layer-inversion symmetry can be proportional to

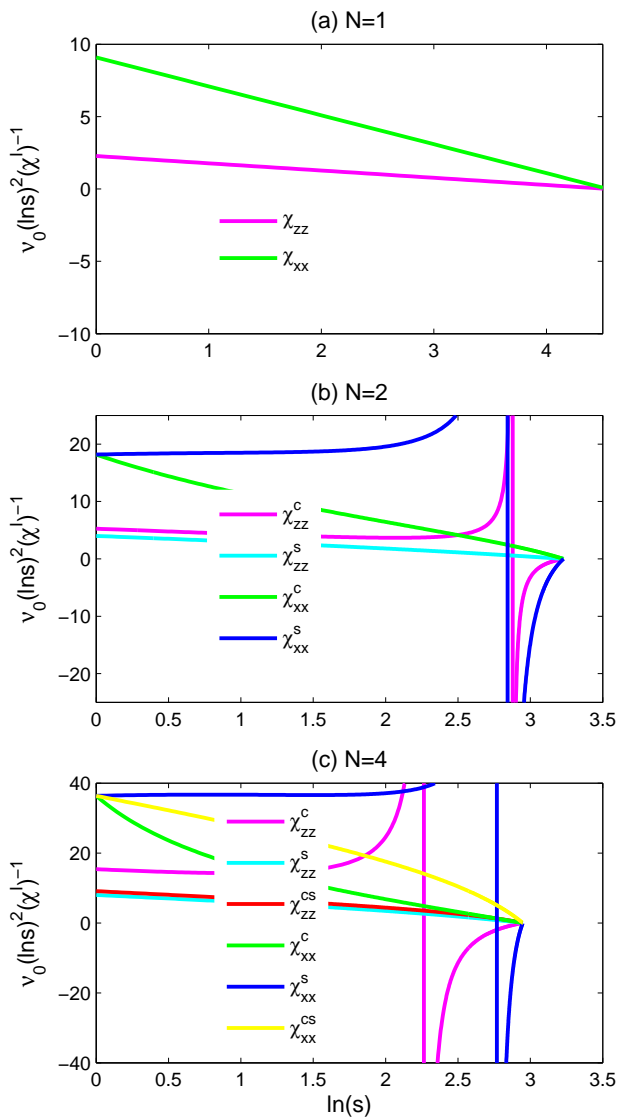


FIG. 7. (Color online) RG flows of interacting susceptibilities for different ordering tendencies. (a) $N = 1$, (b) $N = 2$ and (c) $N = 4$. We use the dimensionless quantity $\nu_0(\ln(s))^2(\chi^T)^{-1}$ in the figures.

$(1 + s^z + \tau^z - s^z\tau^z) \sigma^z/2$. This gapped state breaks parity inversion and time reversal symmetries, favored by small interlayer electric and magnetic fields^{5,13} that break $SU(4)$ symmetry. The difference between this state and other spontaneously broken symmetry states can be further appreciated as follows in our full model with *approximated* $SU(4)$ symmetry. This state reduces the full symmetry to $SU(3) \times SU(1) \times U(1)$ with three Goldstone modes, in contrast to the three possible states in flavor spin channel that break the symmetry down to $SU(2) \times SU(2) \times U(1)$ with four Goldstone modes, and there is no soft mode in the flavor charge channel.

V. DISCUSSION

In this paper we have attempted to shed light on the pseudospin ferromagnet ground state of BLG by carrying out a conventional perturbative renormalization group calculation for a model with $SU(4)$ invariance in spin-valley space, and examining interaction corrections to spin and charge pseudospin susceptibilities. The PRG flows lead to strong layer interchange scattering processes which favor gapless nematic ($\hat{x} - \hat{y}$ -plane pseudospin ferromagnet) ground states, competing with the gapped (\hat{z} -direction pseudospin ferromagnet) states favored by intra-flavor exchange interactions and predicted⁶ by mean field theory. The role of exchange is especially dominant in the single-flavor $N = 1$ case in which the PRG flow equations lead to divergent interactions which vanish when projected onto the many-fermion Hilbert space. For $N = 1$ the interactions enter observable only in the combination $\Gamma_{DS} = \Gamma_D - \Gamma_X$ that is uniquely allowed by the Pauli exclusion principle.

We conclude that the most likely ground states are gapped spin-channel Ising pseudospin ferromagnets, in agreement with some¹²⁻¹⁴ recent experiments, although the competition becomes closer when the number of flavors is larger, and quite close for the physically relevant $N = 4$ case. According to our estimates, broken symmetry states appear at energy scales slightly larger than those at which trigonal warping effects in the single-particle Hamiltonian² start to have a large influence on the band structure, splitting the vorticity $J = 2$ vortex of the chiral model into four $J = 1$ Dirac points. The strength of our conclusions is limited by our neglect of the long-range character of Coulomb interactions and by the fact that our one-loop PRG calculations become unreliable once the effective interactions flow to strong values, *i.e.* once $\nu_0\Gamma \gtrsim 1$.

The details of our calculations are conventional and in particular evaluate the loop corrections to scattering amplitudes for the case in which both incoming and outgoing momenta are at the Dirac point. This simplification is normally justified by the irrelevance of gradient corrections to the effective interactions. As we now explain, in the case of BLG, this approximation likely overestimates the strength of the Γ_X layer interchange interactions. Consider for example the ZS process which is non-zero because of the triplet layer off-diagonal contribution to the Green's functions, as we have approximated in Eq.(8). When the incoming electrons have finite momenta \mathbf{k} and \mathbf{p} , the momentum arguments of the virtual states in the loop diagram are $\mathbf{k} + \mathbf{q}$ and $\mathbf{p} + \mathbf{q}$. The triplet propagator phase factors which are integrated over \mathbf{q} in the loop correction to Γ_X therefore becomes $e^{\pm 2i\theta}$ where $\theta = \phi_{\mathbf{k} + \mathbf{q}} - \phi_{\mathbf{p} + \mathbf{q}}$. Notice that this phase factor has a singular dependence on \mathbf{k} and \mathbf{p} at small \mathbf{q} and that the approximation we have used previously, in which we replace θ by zero, is valid only for $q \gg p, k$. When the phase factors are taken into account the Γ_X scattering amplitude has an additional phase factor which will average

to a value smaller than one in physical observables like the pseudospin susceptibilities. It therefore appears to us that our calculation likely overestimates the strength of the interactions which favor the nematic state.

The gapped states have the interesting property that they support large momentum space Berry curvatures,^{5,50} which can lead to interaction-induced quantum Hall effects. The regions of momentum space near both K and K' valleys flavor contribute $\sim \pm e^2/h$ to the Hall conductivity for each spin. When all flavors make a contribution of the same sign, the total Hall conductivity is exactly $\pm 4e^2/h$. This gapped bilayer state is therefore a quantized anomalous Hall (QAH) insulator^{5,21,50,51} with chiral edge states. Because of its nontrivial overall orbital moment⁵ the QAH state is favored by a perpendicular magnetic field. The state in which the sense of layer polarization is opposite for opposite spins and for opposite valleys does not break time-reversal symmetry and has a mean-field interaction terms with an effective spin-orbit coupling⁵² that leads to a quantum spin Hall (QSH) state with zero charge Hall conductivity. The QSH state has helical edge states protected by time-reversal symmetry. Its \mathcal{Z}_2 classification in an interacting N -layer chiral graphene is given by⁵ $\nu = N \bmod 2$. When lattice effects²³ are taken into account, inter-valley exchange weakly favors the layer-antiferromagnet (LAF)⁵ state. (That observation does not definitively make the case for this particular state, since inter-valley exchange could be less important than correlation effects.) For a LAF state, $\sigma_H = 0$ even though time-reversal symmetry is broken by opposite spin polarizations on the top and bottom layers. In a continuum model that neglects lattice effects and has $SU(4)$ symmetry, the three states are all members of the continuous family of degenerate broken symmetry states that is signaled by divergence of χ_{zz}^s .

In addition to their difference in edge state properties, the QAH, QSH and LAF states also exhibit different responses²⁶ to Zeeman fields which couple to spin and can be realized in the absence of orbital coupling by applying magnetic fields parallel to graphene layers. In the QAH case, the ground state is unchanged but the quasiparticle gap is reduced, vanishing when the Zeeman-coupling strength is equal to the ground state gap via a mechanism reminiscent of the Clogston limit in superconductors. The QSH and LAF states respond to Zeeman fields by establishing noncollinear spin states within each valley and evolving toward an unusual kind of exciton condensate in the strong Zeeman-coupling limit. The quasiparticle gap of QSH and LAF states is however independent of Zeeman-coupling strength drawing a sharp distinction with the QAH case. It is therefore possible to use Zeeman responses and edge state signatures to identify the character of the bilayer ground state experimentally.²⁶ On the other hand, the three states respond very similarly to an electric field between the layers, which can induce first order transitions at which the total layer polarization jumps.^{14,26} This state favored by an inter-

layer electric field is a quantum valley Hall state with zero Hall conductivity but, in the absence of scattering which mixes valleys counterpropagating valley-resolved edge states. We note that a small electric field between the layers can also possibly stabilize a state in which one flavor is polarized in a sense opposite to the other three and charge, valley, and spin Hall conductivities are all nonzero.⁵

One consequence of the above mentioned spontaneous quantum Hall effects⁵ in each valley is that the gapped states have a very simple adiabatic evolution with magnetic field B in which the gap remains open, but the carrier density at which the gap appears varies with field. The total filling factor inside the gap at finite B is ν for a state with a Hall conductance equal to $\nu e^2/h$ at zero field. The topological character⁵ of the gapped states in BLG is induced⁸ by weak bare electron-electron interactions and is enhanced by the nearly flat bands with chiral pseudospin textures, and is distinct from the \mathcal{Z}_2 topological insulators⁵²⁻⁵⁴ that require strong intrinsic spin-orbital coupling. Although interaction-induced topological states apparently do not occur in single-layer graphene, as proposed⁵⁵ on the basis of extended Hubbard models with at least finite interaction strength, it appears quite possible that they do occur in bilayers via a weak interaction instability.⁸

There are three previous articles^{8,17,22} which discuss similar RG calculations. Ref. 17 reports equivalent RG flow equations for the $SU(4)$ invariant model in terms of interaction parameters that are related to ours by $g_{0,z} = \Gamma_S \pm \Gamma_D$ and $2g_{\perp} = \Gamma_X$. Several references have started their RG flows from effective interactions which include symmetry-allowed corrections due to lattice effects. Ref. 22 attempts to account for the long-range of the Coulomb interaction by explicitly accounting for screening and then replacing the Coulomb amplitude by an average value, and estimates the ground state by applying mean-field theory to interactions from PRG flows that have been truncated at an intermediate interaction strength. All calculations recognize the competition between nematic and gapped states, but small differences in approximations or in estimates of bare coupling parameters have led to different final conclusions. We note that the recent elaborations^{20,34} of the calculations which motivated nematic state proposals^{17,22} recognize that gapped states⁸ are also a possibility.

Although these calculations, like ours, shed light on the physics at play in determining the ground state, it is difficult to make definitive conclusions based on theory alone and we must ultimately appeal to experiment. Here the situation is also confusing. Some experimental studies¹²⁻¹⁴ of high-quality suspended bilayers appear to reveal gaps whose size, carrier-density-dependence, and temperature-dependence, is roughly consistent with mean-field-theory predictions.^{14,36} These observations are consistent with the conclusions of this paper. On the other hand this behavior is not observed in all samples, even in samples which appear to be sim-

ilar to the gapped samples. One experimental study¹¹ focuses on the magnetic-field B dependence of the gap at filling factor $\nu = 4$ in a sample which does not show a gap at $B = 0$. The anomalous weak B persistence of the $\nu = 4$ gap in this experiment appears to be consistent with earlier studies by Yacoby and collaborators.^{9,10} Although interpreted as evidence for the nematic study, the persistence of the $\nu = 4$ gap is, it appears to us, equally consistent with a field-driven crossover or transition to a gapped $\sigma_H = 4e^2/h$ state. Although this gap is likely not the ground state at $B = 0$ it is favored at filling factor $\nu = 4$, because its gap is then pinned to the Fermi level. In this interpretation the increased conductance observed at weak fields in Ref. 11 would be associated with a first order transition^{14,35} between $\sigma_H = 4e^2/h$ and $\sigma_H = 0$ states which induces a network of current-supporting⁵⁶ domain walls.²⁴

Similar spontaneously broken symmetry physics⁸ is also likely in thicker high quality graphene films with chiral (ABC) stacking order.^{5,43} In an N -layer chiral stack,⁴ the low-energy sublattice sites are localized in the outermost layers, A_1 and B_N . Hopping occurs between these two sites via an N -step virtual process which leads to p^N energy dispersions and an $N\pi$ Berry phase. For larger N , the low-energy bands are increasingly flat and the pseu-

dospin chirality larger, at least when weak remote hopping processes are neglected, leading to larger opening for many-body interaction effects. In the simplified chiral model, the density of states $D(E) \sim E^{(2-N)/N}$ diverges as E approaches zero for $N > 2$ whereas it remains finite for $N = 2$. In the PRG language, this difference corresponds to the fact that the short-range interactions at tree level are marginal for $N = 2$ but relevant for $N > 2$. Since $V_X = 0$ at tree level, as discussed in Section III-C, it seems that gapped spontaneous quantum Hall states⁵ which break layer-inversion symmetry and produce large momentum space Berry curvatures can occur in multilayers as well. Future experimental and theoretical work will be necessary to sort out the competition between interactions and remote hopping terms in the Hamiltonian.

VI. ACKNOWLEDGEMENTS

FZ has been supported by DARPA under grant SPAWAR N66001-11-1-4110. AHM acknowledges valuable discussions with Joel Moore on the charge and spin susceptibilities of $SU(4)$ invariant systems. AHM was supported by Welch Foundation grant TBF1473, NRI-SWAN, and DOE Division of Materials Sciences and Engineering grant DE-FG03-02ER45958.

* zhf@sas.upenn.edu

¹ A. H. Castro Neto *et al.*, Rev. Mod. Phys. **81**, 109 (2009).

² E. McCann and V. I. Fal'ko, Phys. Rev. Lett. **96**, 086805 (2006).

³ H. Min and A. H. MacDonald, Phys. Rev. B **77**, 155416 (2008).

⁴ F. Zhang, B. Sahu, H. Min and A. H. MacDonald, Phys. Rev. B **82**, 035409 (2010).

⁵ F. Zhang, J. Jung, G. A. Fiete, Q. Niu and A. H. MacDonald, Phys. Rev. Lett. **106**, 156801 (2011).

⁶ H. Min, G. Borghi, M. Polini and A. H. MacDonald, Phys. Rev. B **77**, 041407(R) (2008).

⁷ We refer here to the valley-projected layer-inversion symmetry. This symmetry is broken in the sense that terms proportional to σ^z are generated by electron-electron interactions in the mean-field continuum theory. Note that this layer-inversion symmetry is different than the parity inversion symmetry with the operator $\mathcal{P} = \tau^x \sigma^x$. The band Hamiltonian of chiral graphene has parity inversion symmetry, as $\mathcal{P}\mathcal{H}_J(\mathbf{q})\mathcal{P}^{-1} = \mathcal{H}_J(-\mathbf{q})$. All the spontaneously gapped states classified in ref. 5 break the valley projected layer-inversion symmetry. However, the quantum anomalous Hall and quantum spin Hall states preserve the parity inversion symmetry.

⁸ F. Zhang, H. Min, M. Polini and A. H. MacDonald, Phys. Rev. B **81**, 041402(R) (2010). Also see the supplementary attached to arXiv:0907.2448 for the complete set of PRG flow equations in the spinful and valleyful case.

⁹ J. Martin *et al.*, Phys. Rev. Lett. **105**, 256806 (2010).

¹⁰ R. T. Weitz *et al.*, Science **330**, 812 (2010).

¹¹ A. S. Mayorov *et al.*, Science **333**, 860 (2011).

¹² F. Freitag *et al.*, Phys. Rev. Lett. **108**, 076602 (2012).

¹³ J. Velasco Jr. *et al.*, Nature Nanotechnology, **7**, 156 (2012).

¹⁴ W. Bao *et al.*, arXiv:1202.3212, to appear in PNAS (2012).

¹⁵ A. Veligura *et al.*, arXiv:1202.1753 to appear in PRB (2012).

¹⁶ K. Sun *et al.*, Phys. Rev. Lett **103**, 046811 (2009).

¹⁷ O. Vafek and K. Yang, Phys. Rev. B **81**, 041401(R) (2010).

¹⁸ R. Nandkishore and L. Levitov, Phys. Rev. Lett. **104**, 156803 (2010).

¹⁹ R. Nandkishore and L. Levitov, Phys. Rev. B **82**, 115431 (2010).

²⁰ O. Vafek, Phys. Rev. B **82**, 205106 (2010).

²¹ R. Nandkishore and L. Levitov, Phys. Rev. B **82**, 115124 (2010).

²² Y. Lemonik, I.L. Aleiner, C. Toke and V.I. Fal'ko, Phys. Rev. B **82**, 201408(R) (2010).

²³ J. Jung, F. Zhang and A. MacDonald, Phys. Rev. B **83**, 115408 (2011).

²⁴ F. Zhang, J. Jung and A. H. MacDonald, J. Phys.: Conf. Ser. **334**, 012002 (2011).

²⁵ M. Trushin and J. Schliemann, Phys. Rev. Lett. **107**, 156801 (2011).

²⁶ F. Zhang and A. H. MacDonald, Phys. Rev. Lett. **108**, 186804 (2012).

²⁷ M. Y. Kharitonov, arXiv:1105.5386 (2011).

²⁸ M. Y. Kharitonov, arXiv:1109.1553 (2011).

²⁹ A. H. MacDonald, J. Jung and F. Zhang, Phys. Scr. **T146**, 014012 (2012).

³⁰ R. E. Throckmorton and O. Vafek, arXiv:1111.2076 (2011).

³¹ M. M. Scherer, S. Uebelacker and C. Honerkamp, arXiv:1112.5038 (2011).

- ³² L. Zhu, V. Aji and C. M. Varma, arXiv:1202.0821 (2012).
- ³³ M. Trushin and J. Schliemann, arXiv:1202.2302 (2012).
- ³⁴ Y. Lemonik, I. L. Aleiner and V. I. Fal'ko, arXiv:1203.4608 (2012).
- ³⁵ D. Tilahun, F. Zhang and A. H. MacDonald, to appear (2012).
- ³⁶ F. Zhang, J. Jung, A. H. MacDonald, J. Velasco, W. Bao and C. N. Lau, to appear (2012).
- ³⁷ Yufeng Liang and Li Yang, under preparation.
- ³⁸ D. C. Elias *et al.*, Nature Phys. **7**, 701 (2011).
- ³⁹ J. Gonzalez, F. Guinea and M. A. H. Vozmediano, Nuc. Phys. B **424**, 595 (1994).
- ⁴⁰ G. Borghi, M. Polini, R. Asgari and A. H. MacDonald, Solid State Commun. **149**, 1117 (2009).
- ⁴¹ Aaron Bostwick *et al.*, Science **328**, 1186489 (2010).
- ⁴² Marco Polini *et al.*, Phys. Rev. B **77**, 081411 (2008); E.H. Hwang, and S. Das Sarma, Phys. Rev. B **77**, 081412 (2008).
- ⁴³ W. Bao *et al.*, Nature Physics **7**, 948 (2011).
- ⁴⁴ Specifically we rotate by 180° around the \hat{y} -axis so that $\sigma_y \rightarrow -\sigma_y$ and $\sigma_z \rightarrow -\sigma_z$. This choice does not change the interaction term in the Hamiltonian, even in models that account for the difference between intralayer and interlayer interactions. It has the advantage of implying the conservation of the \hat{z} component of layer pseudospin that is used to simplify our diagrammatic calculations. However, we do have to remember to invert the transformation when we interpret the layer interchange interaction Γ_X which appears in our calculations. The inter-valley Γ_X scattering process is actually one in which two electrons in the same layer are both scattered to the opposite layer. It is of course possible to perform our calculations without making this transformation simply by replacing ϕ by $\pi - \phi$ in Eq.(5) for valley K' .
- ⁴⁵ E. McCann and M. Koshino, Phys. Rev. B **80**, 165409 (2009).
- ⁴⁶ F. Zhang, D. Tilahun and A.H. MacDonald, Phys. Rev. B **85**, 165139 (2012).
- ⁴⁷ R. Shankar, Rev. Mod. Phys. **66**, 129 (1994).
- ⁴⁸ T. Giamarchi, *Quantum Physics in One Dimension* (Clarendon Press, Oxford, 2003).
- ⁴⁹ Y. Q. Li, Michael Ma, D. N. Shi, and F. C. Zhang, Phys. Rev. Lett. **81**, 3527 (1998) and work cited therein.
- ⁵⁰ D. J. Thouless, M. Kohmoto, M. P. Nightingale, and M. den Nijs, Phys. Rev. Lett. **49**, 405 (1982).
- ⁵¹ F. D. M. Haldane, Phys. Rev. Lett. **61**, 2015 (1988).
- ⁵² C. Kane and E. Mele, Phys. Rev. Lett. **95**, 226801 (2005).
- ⁵³ M. Z. Hasan and C. L. Kane, Rev. Mod. Phys. **82**, 3045 (2010).
- ⁵⁴ X. Qi and S. Zhang, Rev. Mod. Phys. **83**, 1057 (2011).
- ⁵⁵ S. Raghu *et al.*, Phys. Rev. Lett. **100**, 156401 (2008).
- ⁵⁶ Z. Qiao, J. Jung, Q. Niu and A. H. MacDonald, Nano Letters **11**(8), 3453 (2011).